Journal of Alloys and Compounds 517 (2012) 139–148

Contents lists available at SciVerse ScienceDirect

Journal of Alloys and Compounds

journal homepage: www.elsevier.com/locate/jallcom

Studies on the synthesis of cubic ZnS quantum dots, capping and optical–electrical characteristics

R. Sakthi Sudar Saravanan [a,*], D. Pukazhselvan [b], C.K. Mahadevan [a]

[a] Physics Research Centre, S.T. Hindu College, Nagercoil 629 002, Tamilnadu, India
[b] Hydrogen Energy Centre, Department of Physics, Banaras Hindu University, Varanasi, India

ARTICLE INFO

Article history:
Received 7 September 2011
Received in revised form
12 December 2011
Accepted 14 December 2011
Available online 23 December 2011

Keywords:
Semiconductors
Microwave synthesis
Quantum dots
Optical bandgap
Electrical conductivity
Activation energy
Thermionic emission

ABSTRACT

This paper presents a comparative analysis of ZnS QDs synthesized by conventional and microwave heating techniques using zinc acetate and sodium sulphide reactants. The size of the quantum dots achieved by the latter technique (~3 nm) is at least 30 times smaller than the former technique. Incorporation of excess Na_2S and microwave treatment are the important factors responsible for controlling the size of ZnS nanocrystals. Furthermore, the distribution of quantum dots is highly influenced by the addition of small amount of NaOH. The UV–vis analysis reveals that the band gap can be widened up to 3.94 eV (correspond to ~3 nm ZnS) from 3.67 eV (correspond to bulk ZnS). Surprisingly better conductivity is observed for the widest band gap ZnS of the present study; this could be due to defects/vacancies present in the system and its influence in the band structure. The higher conductivity value is supported by the smaller activation energy value, smaller dielectric constant and higher dielectric loss, etc. The conduction is further explained by thermionic emission mechanism.

1. Introduction

In recent years much attention has been paid to II–VI compound semiconductors because of their potential applications in optoelectronics. The importance of these candidates in device fabrication has also been extensively demonstrated by many researchers. As for example, UV light emitting diodes [1], blue light emitting diodes [2], emissive flat screens [3], quantum dot lasers [4] and solar cells [5], etc. One of the striking properties of II–VI semiconductors is that, tunable optical properties can be achieved by modulating their size, chemical composition and defect concentration, etc. [6]. Therefore developing suitable material tailoring and processing techniques is a significant part of research in this area. Most of the well known synthesis methods in present time need higher temperatures and strict inert ambient [7]; this makes these synthesis methods much cost intensive. It is therefore necessary to explore simpler and more convenient strategies to produce property tunable quantum dots.

Among the II–VI compound semiconductors, zinc sulphide (ZnS) is particularly an interesting candidate because of its large and direct bandgap (3.65 eV at room temperature). ZnS quantum dots (QDs) have recently been shown to have potential properties for energy production [8] and biomedical applications [9]. The variation of optical/electrical property of ZnS as a result of tailoring the geometry has now become a widely known phenomenon. By measuring the variations of energy gap (E_g), dielectric constant (ε_r), dielectric loss ($\tan\delta$), electrical conductivity (σ_{ac} and σ_{dc}) and activation energy for conduction (ΔE) with respect to the size of particles, useful insights regarding the mechanism of conduction can be made for this system. Recent reports reveal that [10,11] the presence of lattice defects/impurity states in band gap significantly alters the conductivity of the sample. Since the activation energy for conduction is significantly reduced by the lattice defects/impurity states in the band gap, the wideband gap semiconductor with defect states can exhibit conductivities similar to narrow band gap semiconductors [12]. In light of this we have synthesized ZnS quantum dots with different size and studied the particle size dependence of all the aforesaid electrical parameters for the system. From these, we tried to throw some light on the mechanism of conduction in the wide band gap – but conducting semiconductors. Porter et al. [13] have studied the dark and photoconduction mechanisms of ZnS crystals and evaporated ZnS films in detail. However, still there is only limited literature knowledge on the size dependence of electrical parameters in ZnS system [14].

Engineering wide band gap semiconductors with better conductivity is a challenging task [15] and such semiconductors hold promising applications in the field of high temperature optoelectronics [16]. Thus, in this work, we report a novel synthesis approach for obtaining electrically conducting wide band gap cubic

* Corresponding author. Tel.: +91 9443483449.
E-mail address: rsakthiss@yahoo.com (R.S.S. Saravanan).

0925-8388/$ – see front matter © 2011 Elsevier B.V. All rights reserved.
doi:10.1016/j.jallcom.2011.12.060

Table 1
Sample codes used for present study and obtained yield percentage of samples.

Sample code	Reactants	Composition ratio of reactants	Capping agent	Heat treatment method	Yield % = (mass of reactants/mass of product) × 100
ZnS(1)	Zinc acetate dihydrate + sodium sulphide	1:1	–	Microwave	23.42
ZnS(2)		1:2	–	Microwave	29.64
ZnS(3)		1:3	–	Microwave	34.73
ZnS(C)		1:3	NaOH	Microwave	26.41
ZnS(B)		1:3	–	Conventional	19.32
ZnS(D)		1:3	NaOH	Conventional	14.81

ZnS QDs by solvothermal-microwave irradiation technique. This is a very simple and cost-effective method for deriving high yield of ZnS QDs with the sizes of <4 nm. Since the as-prepared materials exist in the form of aggregates of particles, we tried a NaOH treatment by which it is possible to extend the particle–particle distance to a better extent. The synthesized materials have been characterized by XRD, SEM, TEM, EDAX, UV–vis spectroscopy and electrical studies (E_g, ε_r, $\tan\delta$, σ_{ac}, σ_{dc}, ΔE and quantum confinement characteristic features). It is observed that changing the ratio of Zn and S bearing precursors from 1:1 to 1:3 with microwave as the heating source leads to reduction of the derived ZnS crystallite size more than a factor 2. The presence of excess Na_2S (sulphur bearing precursor) plays a major role as a size modulator. The microwave assisted heating is found to be a far effective method as compared to the conventional heating method. QDs of size ~3 nm could be achieved by microwave assisted solvothermal method which is otherwise >100 nm by conventional heating assisted solvothermal method. The size reduction of QDs to ~3 nm leads to widening of the band gap of this material to a greater extent (3.944 eV from 3.64 eV). The activation energy for conduction has been found to decrease with the decrease in the size of the QDs. Thus, in spite of their wide band gap better conductivity is observed. This is, in this respect, one of the better results observed so far. The quantum confinement features of the optimum material (crystallite size to bohr exciton radius ratio <1) have also been described and the mechanism of conduction is attributed to thermionic emission of charge carriers from grain boundaries.

2. Experimental procedure

2.1. Synthesis of ZnS nanocrystals

Analytical reagent (AR) grade zinc acetate dihydrate ($Zn(CH_3COO)_2{\cdot}2H_2O$), and sodium sulphide ($Na_2S$) were purchased from Merck Chemicals. These compounds were used without further purification for the preparation of ZnS. Zinc acetate dihydrate is mixed with sodium sulphide in 1:1, 1:2 and 1:3 molecular ratios. The fine mixture was then dissolved in 100 ml doubly distilled water with vigorous stirring for 30 min at room temperature. As soon as the mixture was dissolved in double distilled water, S^{2-} starts combining with Zn^{2+} to become ZnS nanocrystals. Therefore treating this as a seed solution, three different approaches have been further employed. In the first case the seed solution was placed in a conventional heater and the solution was heated just above the boiling point. Heating was performed until the solvent evaporates completely and the whitish ash powder was collected as yield. In the second case the seed solution was heated using a microwave oven under similar condition until the solvent evaporates completely. In the third case 0.5 M NaOH solution was slowly added into the seed solution and stirred by a magnetic stirrer at the temperature of 50 °C for 30 min. This material was then transferred to microwave heater (for comparison, third case was also performed by conventional heater). Thus, four different ways of sample preparation is adopted for the present study such as (i) convention heating without NaOH treatment (ii) conventional heating with NaOH treatment (iii) microwave heating without NaOH treatment and (iv) microwave heating with NaOH treatment. The microwave irradiation was performed with the frequency of 2.45 GHz and 800 W power. For the further information regarding microwave irradiation treatment the reader is referred to our earlier report [17]. The colloidal precipitate obtained at the end was cooled to room temperature naturally and washed several times with doubly distilled water and then with acetone to remove the impurities and unintended reaction products. The sample was then filtered and dried in an oven with controlled heating condition at 60 °C for 48 h to remove the volatile impurities and collected as the yield. All the as-prepared powder samples were again annealed at 150 °C using a programmable furnace for 2 h. Temperature ramp was fixed to 5 °C/min with the accuracy of ±0.5 °C. The mass of the samples was measured accurately and yield percentage was calculated. The codes used to describe the samples and yield percentage of the samples are summarized in Table 1.

2.2. Structural/microstructural characterization

X-ray powder diffraction patterns were obtained using an automated PANalytical X-ray powder diffractometer with monochromated CuK_α radiation (λ = 1.54056 AU). The crystallite size analysis was made using Scherrer [18] and Voigt function methods [19]. The volume fraction of interfaces (V_{if}), grain boundaries (V_{gb}) and triple junctions (V_{tj}) with respect to the total volume of the particles are calculated using the method as described by Palumbo et al. [20]. Microstructural analysis has been performed using SEM Zeiss-SUPRA 40 by secondary electron imaging mode. The particle size analysis of the as-synthesized material has been carried out using TEM-FEI Technai G^2 300 kV. The lattice constant '*a*' for the cubic phase of ZnS is determined by Rietveld refinement technique [21]. Energy dispersive X-ray analysis (EDAX) was used to estimate the composition of the materials using EDX-System OXFORD INCA Energy 200.

2.3. Optical measurements

Optical absorption measurements were done at room temperature using a SHIMADZU UV-2400 PC spectrometer with a medium scan speed sampling interval of 0.5 nm in the wavelength range of 250–600 nm. The fundamental absorption, which corresponds to electron excitation from the valence band to conduction band, can be used to determine the value of the optical bandgap. The absorption coefficient α was determined using the relation,

$$\alpha = \frac{2.303\ \log(\text{absorption})}{\text{Thickness of the sample}}. \quad (1)$$

The relation between the absorption coefficient (α) and the incident photon energy ($h\upsilon$) can be written as [22]:

$$(\alpha h\upsilon) = A(h\upsilon - E_g)^n, \quad (2)$$

where, A is a constant, E_g is the bandgap energy of the material and exponent n depends on the type of transition [23]. Here, the transitions are direct so we take $n = 1/2$.

2.4. Electrical measurements

The resultant powder material prepared in the present study was compacted into disc shaped pellets of dimensions 8 mm in diameter and 1.5 mm (±0.15 mm) in thickness with 4 t hydraulic pressure. The dimensions of the pellets were measured using a travelling microscope (L.C. = 0.01 mm). Prior to any measurements, the pelletized samples were again annealed under controlled heating conditions for 30 min at ~150 °C to achieve densification. After this, both surfaces of the sample were coated with silver paste to obtain a good conductive surface layer. The capacitance (C) and dielectric loss factor ($\tan\delta$) measurements were carried out to an accuracy of ±1% with Agilant 4284A LCR meter in the temperature range of 40–130 °C. The observations were made while cooling the sample by using the conventional two-probe technique [19]. Temperature was controlled to an accuracy level of ±0.5 °C. The air capacitance (C_{air}) in between the two electrodes was also measured. The dielectric constant (ε_r) of the crystal was calculated using the relation,

$$\varepsilon_r = \frac{C}{C_{air}}. \quad (3)$$

The AC electrical conductivity (σ_{ac}) was calculated using the relation

$$\sigma_{ac} = \varepsilon_o \varepsilon_r \omega\ \tan\delta, \quad (4)$$

where ε_o is the permittivity of free space (8.854×10^{-12} F/m) and ω is the angular frequency ($\omega = 2\pi f$; f = 1 kHz in the present study). The resistances of the pellets were measured using a HP 3457A digital multimeter (Resistance range: 30 Ω to 3 GΩ). The DC conductivity (σ_{dc}) of the crystal was calculated using the relation

$$\sigma_{dc} = \frac{d}{RA} \quad (5)$$

where, R is the measured resistance, d is the thickness of the sample and A is the area of the face in contact with the electrode. The activation energy (ΔE) for conductivity [24] (both AC and DC) has been calculated from the Arrhenius relation,

$$\ln \sigma = \ln \sigma_o - \frac{\Delta E}{kT} \quad (6)$$

where, T is the absolute temperature, k is the Boltzmann constant and σ_o is a constant.

3. Results and discussion

3.1. Structural studies

Synthesis of zinc sulphide can be achieved in both cubic and hexagonal phases. In our previous report [17] we had shown the synthesis of hexagonal Zn_xCd_yS QDs with and without Mn^{2+} dopant. In the present investigation, we discuss the synthesis of cubic ZnS quantum dots by microwave heating of zinc acetate dihydrate and sodium sulphide reactants. Reaction was carried out under distilled water medium for three different ratios of zinc acetate dihydrate and sodium sulphide reactants such as, 1:1, 1:2 and 1:3 (the codes given for these three samples are ZnS(1), ZnS(2) and ZnS(3)). The corresponding XRD patterns are given in Fig. 1. Comparison of XRD data with the standard JCPDS source for the ZnS reveals a fairly well cubic structure with lattice parameters closer to the standard values. As seen, the Rietveld refined pattern makes a closer fit with the observed powder pattern. The refined unit cell parameters are given in Table 2. Careful peak profile analysis (ZnS (1 1 1), see the inset of Fig. 1) indicates that, as we change the ratio of Zn acetate and sodium sulphide from 1:1 to 1:3, there is not only significant change in the integral breadth of the pattern but also a tangible shift in the peak position. The regular right shift indicates the reduction of lattice parameter of ZnS structure. The average crystallite size of ZnS nanocrystals is calculated from the width of ZnS (1 1 1) peak at half maximum intensity and integral breadth (area/height) of the peak using Scherrer and Voigt methods. The calculated crystallite sizes using both Scherrer method and Voigt function method are given in Table 2. The crystallite size value varies from ~6 nm to 1.6 nm when the reactant ratio is changed from 1:1 to 1:3.

The heating technique influences the size and lattice structure of the ZnS crystals to a significant extent. In order to illustrate this, in Fig. 2 we have given the XRD of the ZnS samples as obtained by both conventional heating (ZnS(B)) and microwave heating techniques (ZnS(3)) for the concentration of 1:3. For both the cases, XRDs of NaOH treated samples are also given (ZnS(D) and ZnS(C)). The observed sharp peaks in the conventional heating employed samples as against the microwave assisted samples particularly with different peak positions envisage the following facts. (i) The smallest crystals can be achieved only by microwave heating. It can be understood from the achieved crystallite size of 1.6 nm for this case against the 31 nm observed for the conventional technique (see Table 2). (ii) Microwave heating not only influences the microstructure but also the crystal structure of the as synthesized material. As can be noticed, the crystal system observed by the conventional heating method is hexagonal and by microwave heating, it is cubic. (iii) In both the conventional and microwave techniques, NaOH treatment does not affect the crystal structure but it influences the size of the grown crystals. It can be understood by comparing the peak width of all the cases shown in Fig. 2. Further data regarding this is summarized in Table 2. Thus, from the above analysis, it can be said that the microwave assisted solvothermal method is a suitable method for the synthesis of QDs.

It is known that incorporation of NaOH tunes the pH value of the reaction media [25,26]. However, it also known that reaction of NaOH with Zn acetate under aqueous media results in the formation of $Zn(OH)_2$ [27] and $Zn(OH)_2$ is known to work as a capping

Table 2
Calculated structural data and crystallite size from powder XRD.

Sample code	JCPDS file no.	Reference parameters (from JCPDS)			Calculated parameters (from Rietveld)		Crystallite size	
		a (Å)	c (Å)	V (Å^3)	a (Å)	V (Å^3)	Scherrer method (nm)	Voigt method (nm)
ZnS	05-0556	5.4060		157.99	–	–	–	–
ZnS(1)	–	–		–	5.4753 (± 0.0034)	164.14 (± 0.31)	7.16 (±0.26)	5.94 (±0.11)
ZnS(2)	–	–		–	5.4131 (± 0.0021)	158.61 (± 0.19)	3.70 (±0.18)	3.12 (±0.13)
ZnS(3)	–	–		–	5.3741 (± 0.0015)	155.21 (± 0.13)	1.97 (±0.16)	1.61 (±0.09)
ZnS(C)	–	–		–	5.3989 (± 0.0012)	157.37 (± 0.10)	3.52 (±0.19)	2.62 (±0.11)

Sample code	JCPDS file no.	Reference parameters (from JCPDS)			Calculated parameters			Crystallite size	
		$a = b$ (Å)	c (Å)	V (Å^3)	$a = b$ (Å)	c (Å)	V (Å^3)	Scherrer method (nm)	Voigt method (nm)
ZnS(B)	36-1450	3.82098	6.2573	79.12	3.8152 (± 0.002)	6.2404 (± 0.003)	78.66 (± 0.12)	34.54 (±1.42)	30.39 (±1.08)
ZnS(D)	–	–	–	–	3.8277 (± 0.018)	6.2544 (± 0.013)	79.36 (± 0.72)	11.01 (±0.72)	9.68 (±0.36)

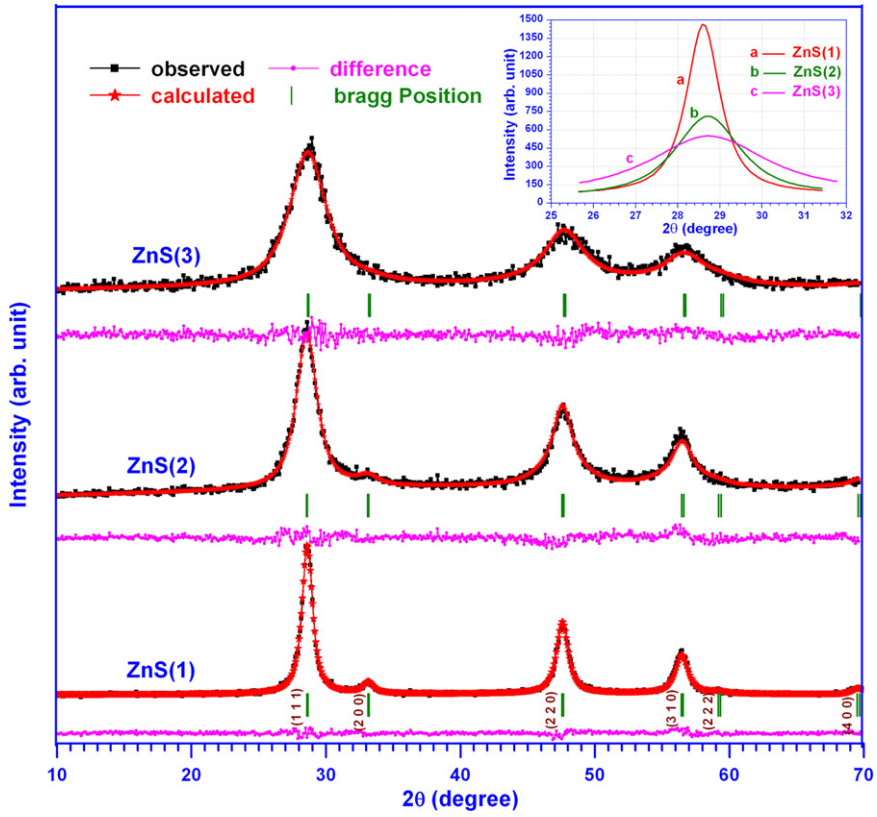

Fig. 1. X-ray powder diffraction pattern and Rietveld refined pattern of the cubic ZnS structure prepared for three different ratio of reactant precursors, 1:1, 1:2 and 1:3 (see sample codes in Table 1). The inset shows the comparison of ZnS (1 1 1) peak of both the three materials. (Colour online.)

agent [28]. Thus, in order to offer such a capping effect we tried NaOH treatment for our samples. It should be noted that NaOH is not added during the starting stage of the reaction. This is otherwise added once we witnessed a significant portion of the reactants have already reacted, so that unwanted reaction pathways could be controlled (as for example, formation of ZnO, etc.). In order to understand whether such treatment indeed play a role in the microstructure, we have carried out SEM study of the ZnS prepared by conventional heating technique (ZnS(B) and ZnS(D)) for the concentration of 1:3. The comparison is shown in Fig. 3. As can be noticed, the NaOH treatment does make an influence in the microstructure and distribution of particles. This may be due to the effect of capping, however since the studied samples are of conventional method (bulk crystals); further HRTEM analysis is required to understand the effect on smaller particles (microwave heated samples). The HRTEM image of the optimum ZnS sample prepared by microwave heating technique (for which the zinc to sulphur reactant concentration is 1:3 ratio) is given in Fig. 4(a). The TEM picture indicates that the dots exist in the form of aggregates of particles with the average dot size of ~3.5 nm. Thus again capping trial (NaOH treatment) was made as an attempt to separate the dots to a possible extent and to prevent the agglomeration of particles. Discussing the experimental runs for the optimum concentration of NaOH is beyond the scope of the present study. Therefore we herewith discuss for only one concentration of NaOH (0.5 mol) employed for ZnS QDs. The TEM images of the capped ZnS QDs are shown in Fig. 4(b) and (c). As seen the NaOH treatment relaxes the individual dots from the aggregates and enhances the distance between individual dots. However, still the dots are coexisting and separating the dots to greater distances more than ~1–2 nm has not been possible.

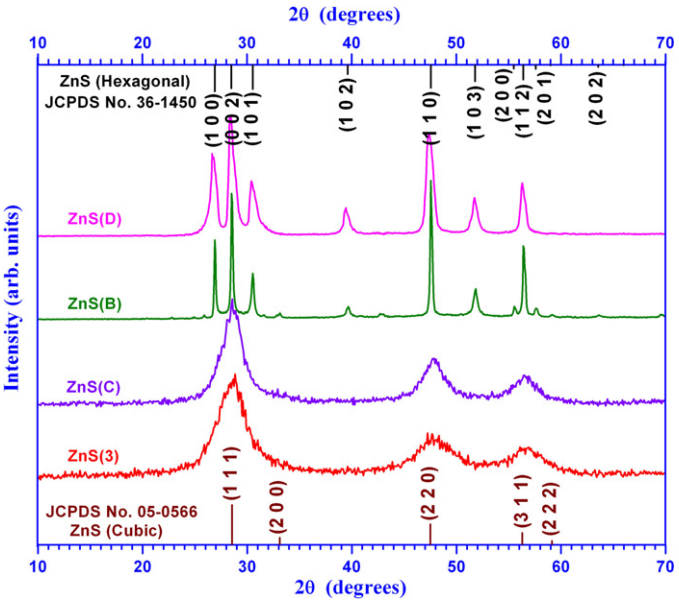

Fig. 2. X-ray powder diffraction pattern for ZnS prepared by conventional method (with and without NaOH treatment) and microwave heating method (with and without NaOH treatment). (Colour online.)

3.2. Role of microwave assisted heating and excess Na_2S on the microstructure of ZnS QDs

The result discussed in the preceding section clearly indicate that heating the zinc acetate and sodium sulphide reactants in 1:3 ratio by microwave heaters, with or without a small amount of NaOH, lead to the formation of ZnS QDs. It is well known that the

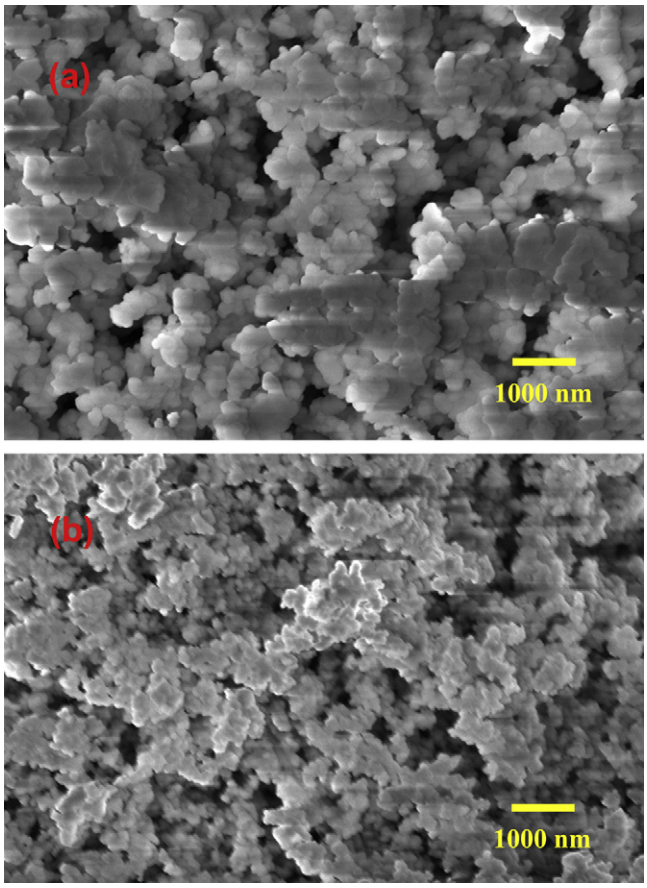

Fig. 3. SEM pictures of ZnS crystals prepared through conventional heating method for the reactant concentration of 1:3. (a) and (b), respectively, represent the derived microstructure without and with NaOH treatment. (Colour online.)

dipoles tend to re-orient under the influence of microwave electric field and cause re-orientation loss in the form of heat [29]. The re-orientation loss originates from the inability of dipoles to follow the extremely rapid reversals of the electric field. Thus, by using microwave source, the heating effect is basically given in molecular level. However, in the present case the question is not just about effective heating but is also about the size reduction of the particles. The exact mechanism of size reduction in the present case is not clearly understood, however we believe that the excess amount of Na_2S play a role as size modulator. It can be understood from the fact that only 1:1 ratio of Zn and S is actually required for the formation of ZnS. It appears to be the excess Na_2S (existing in 1:2 and 1:3 ratio of reactants) helps to reduce the size of ZnS crystals through its interaction with ZnS seed crystals under rapidly re-orienting conditions. Recently, Xiong et al. [30] have investigated CdS system and observed that the addition of Na_2S significantly influences the structure and crystallite size of CdS nanocrystals. They concluded that Na_2S interacts with the CdS surface and takes part in interfacial nucleation. In another study on CdTe system, Liu et al. [31] have reported that addition of Na_2S significantly influence the optoelectronic characteristics of the CdTe nanocrystals. They have identified that the sulphur anions of Na_2S is attracted by Cd cations and even results in the formation of CdS in smaller amount. From these insights we believe that, the seed crystals of ZnS are initially encapsulated by Na_2S due to the attractive interaction between S anions of Na_2S with the Zn cations of ZnS. When higher amount of Na_2S presents, the contact surfaces of neighboring ZnS get dominantly interrupted by Na_2S and their continuous re-orientation due to microwaves may not allow the particles to weld each other.

Table 3
Summary of material composition (at.%) obtained using EDAX.

Sample code	Material composition (at.%)	
	Zinc	Sulphur
ZnS(1)	50.88	49.12
ZnS(2)	47.61	52.39
ZnS(3)	43.47	56.53

When we further heat the system under air medium until the solution evaporates completely, possibly there could be formation of NaOH, H_2S and sulphur deposits. The presence of sulphur is confirmed from EDAX analysis and the release of small amount H_2S is also confirmed from the rotten egg smell experience during the synthesis process. NaOH is known to offer capping of the ZnS surfaces by forming $Zn(OH)_2$ layer and this along with other unintended byproducts can be removed by the two step purification at the end of the process. Thus, employing excessive Na_2S, in a way controls the growth and even offer capping effect for ZnS quantum dots.

The XRD analysis indicated that, at the concentration of Zn and S bearing precursor in 1:1 ratio, comparatively bigger size of ZnS is derived. The smallest dot size has been observed for the precursor concentration of 1:3 ratio. So it is expected that excess sulphur or sulphur bearing compounds exists as a secondary phase; however, XRD analysis did not reveal any signature of excess sulphur. The absence of XRD peaks of sulphur indicates that sulphur should be either in XRD amorphous phase or it might have got lost by microwave irradiation treatment. In order to explore the latter possibility we have subjected all the three products to EDAX analysis. Fig. 5 shows the EDAX spectrum of ZnS nanocrystals such as ZnS(1), ZnS(2) and ZnS(3). The nearly similar Zinc to sulphur atomic ratio observed for ZnS(1) shows (see Table 3) the product is stoichiometric. The presence of excess S for ZnS(2) and ZnS(3), as compared to ZnS(1) clearly shows that excess sulphur indeed presents without getting wiped out by the microwave treatment. From these observations it is reasonable to presume that the QDs are actually embedded in X-ray amorphous sulphur matrix and is beneficial for keeping the dots intact.

3.3. UV–vis spectral studies

Fig. 6(a) shows the observed optical absorption spectra for the samples such as ZnS(1), ZnS(2) and ZnS(3). The corresponding energy vs $(\alpha h\upsilon)^2$ plot is given in the inset. The observed optical bandgap energy values vary from 3.738 to 3.944 eV. More importantly, the observed bandgap energies for all the three quantum dots are significantly higher as compared to the bulk ZnS (3.65 eV) (also see Fig. 6(b)) [32]. Fig. 6(b) brings out the comparison of UV–vis spectrum observed for the samples prepared by conventional heating (ZnS(B)), and the samples prepared by microwave heating method (both the samples, with and without NaOH treatment are given, i.e. ZnS(C) and ZnS(3)). As seen the (bulk) band gap of 3.67 eV was enhanced to 3.94 eV. The band gap observed for the NaOH treated ZnS (ZnS(C)) is slightly lower (3.89 eV) than that observed for ZnS(3). It may be due to the fact that the gross particle size of ZnS(C) is slightly bigger than ZnS(3). Thus, from the comparative features of both Fig. 6(a) and (b), it can be said that the increase in bandgap energy is a result of reduction in the particle size. The variation of absorption edge and bandgap values with respect to the different reactant ratios is summarized in Table 4. The observed blue-shift increases with the decrease in the particle and crystallite size of ZnS QDs.

We have also observed that the as-prepared ZnS offers strong quantum confinement effect. For detailed description regarding the simple analysis of quantum confinement effects of semiconductor structures, the reader is referred to our previous report [19]. It is

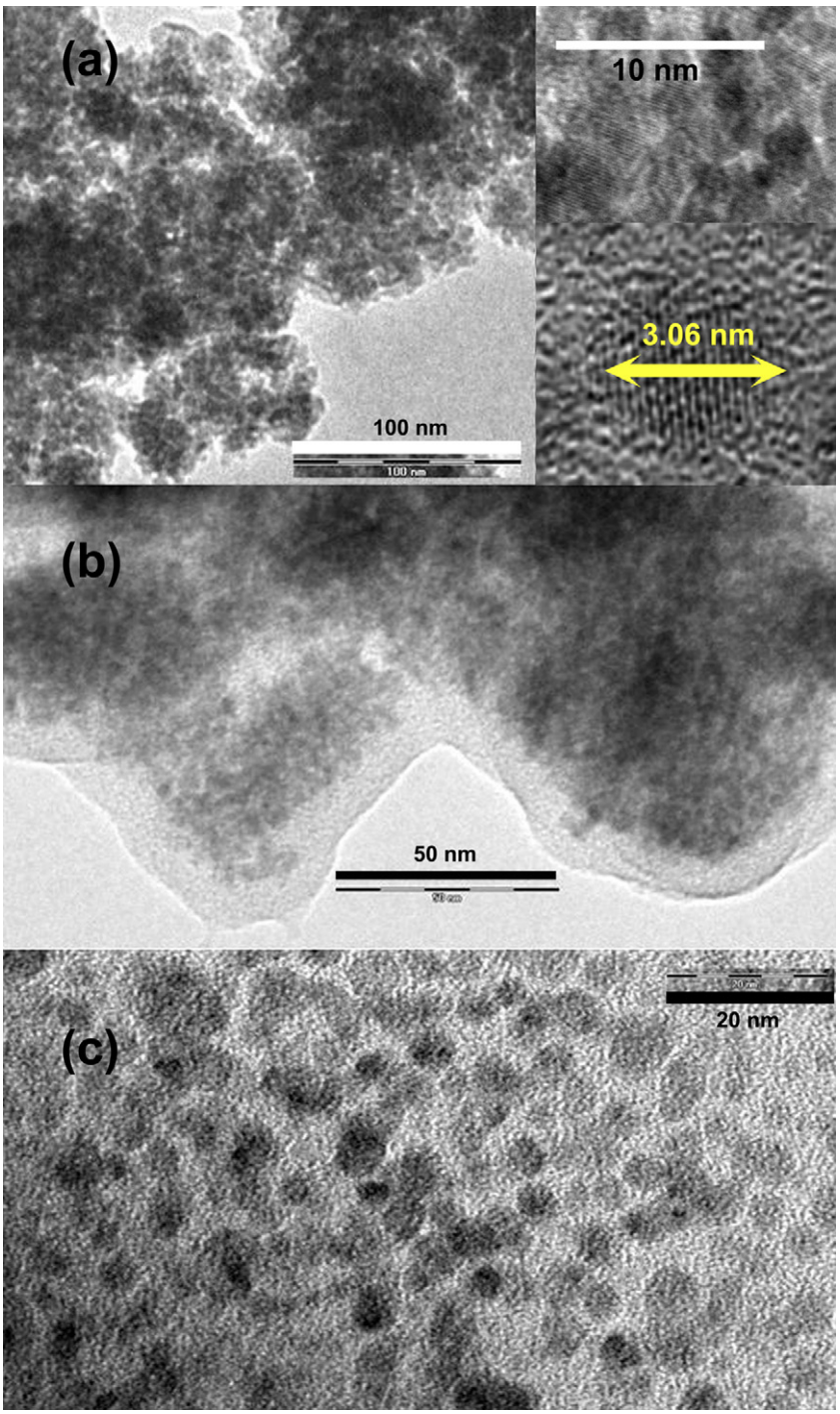

Fig. 4. TEM image of ZnS QDs (ZnS(3) & ZnS(C)) prepared for the zinc acetate to sodium sulphide reactant concentration of 1:3 ratio by solvothermal-microwave irradiation technique: (a) before NaOH treatment. Inset shows the HRTEM image (b) after NaOH treatment and (c) a magnified portion of image of 'b' indicating the fine dispersion of QDs as a result of NaOH treatment. (Colour online.)

known that semiconductor nanocrystals with crystallite size significantly smaller than the exciton Bohr radius shows size-dependent optical properties due to the strong quantum confinement effect for the charge carriers. A weak quantum confinement effect occurs when the crystallite size is larger than the Bohr radius [33]. It is known that the typical exciton Bohr radius for ZnS is 3 nm [34]. Only very few reports have so far been known with crystallite size lesser than or closer to the exciton Bohr radius of ZnS. The calculated crystallite sizes for ZnS(1), ZnS(2), ZnS(3), ZnS(C) and ZnS(B), respectively, 5.94, 3.12, 1.61, 2.62 and 30.39 nm. Thus, the ZnS(1), ZnS(C) and ZnS(B) nanocrystals appear to exhibit weak quantum confinement and ZnS(3) nanocrystal offers strong quantum confinement characteristics.

3.4. Electrical characteristics

It is known that the electrical behavior of nanostructured materials is strongly influenced by geometrical factors [35]. Fig. 7(a)–(d) shows the temperature dependence of electrical parameters such as ε_r, $\tan\delta$, σ_{ac} and σ_{dc} observed in the present study for the

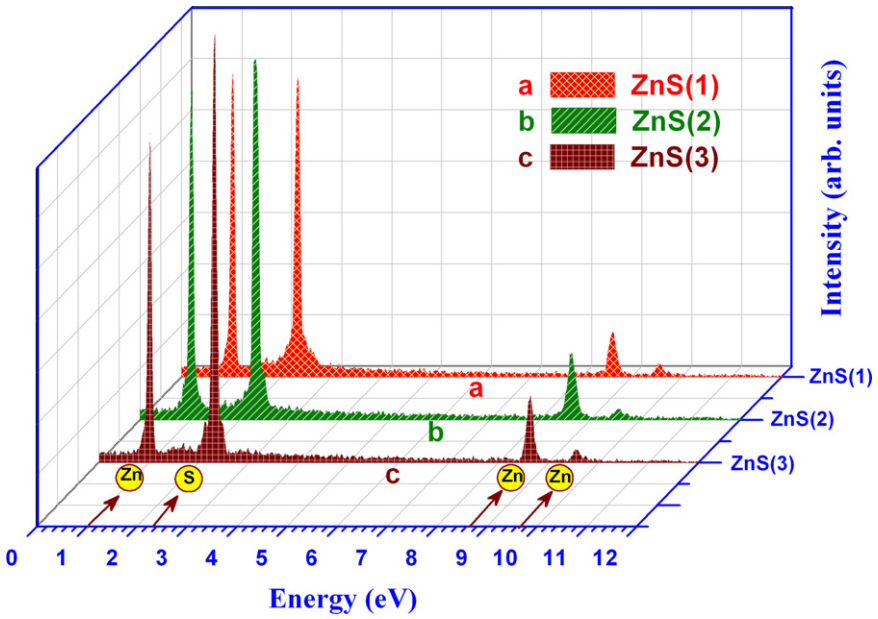

Fig. 5. EDAX spectrums of the as-prepared materials using the reactants zinc acetate to sodium sulphide in (a) 1:1 ratio, (b) 1:2 ratio and (c) 1:3 ratio. (Colour online.)

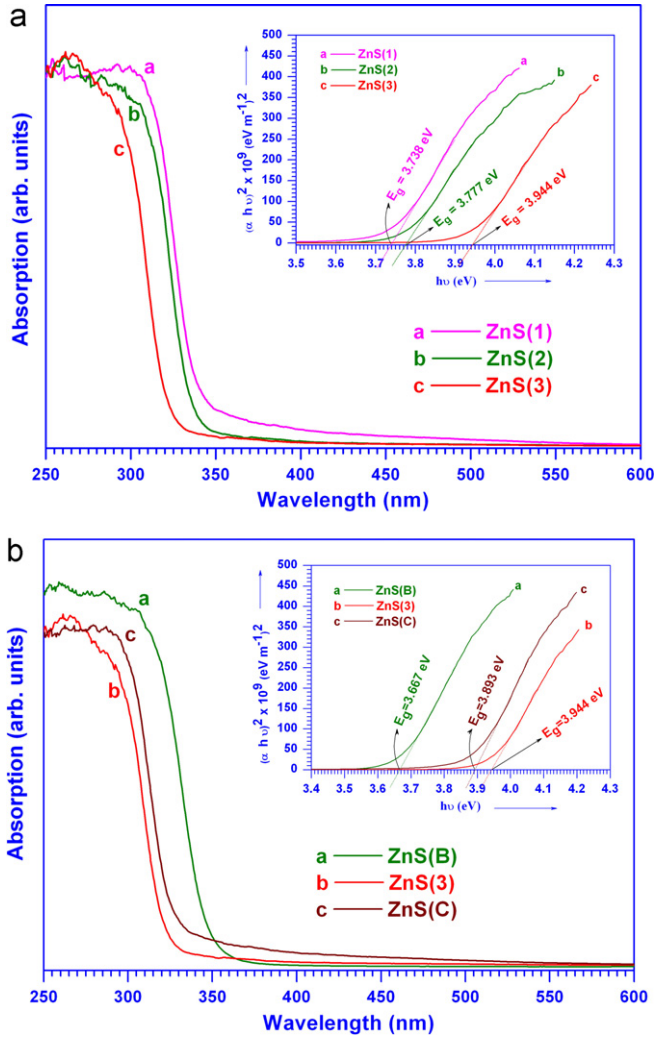

Fig. 6. (a) UV–vis spectrum of ZnS quantum dots ZnS(1), ZnS(2) and ZnS(3), (b) UV–vis spectrum of ZnS(B), ZnS(C) and ZnS(3). The inset shows the determination of optical bandgap energies for the respective samples. (Colour online.)

temperature range of 40–130 °C at a constant frequency (1 kHz). It can be seen that all the four electrical parameters increase with the increase in temperature. From the nature of curves shown in Fig. 7(a) and (b), it is clear that, as the size of ZnS decreases the dielectric constant ε_r decreases and the dielectric loss factor $\tan\delta$ increases (see the Table 2 for comparing the crystal size for the concerned materials). From the relation given in (4), it is clear that the observed ε_r and $\tan\delta$ values would result in higher conductivity and is expected to be in the series of ZnS(3) > ZnS(C) > ZnS(2) > ZnS(1) > ZnS(B). Exactly the same trend is observed in the σ_{ac} and σ_{dc} conductivities (see Fig. 7(c) and (d)). In all the cases, σ_{ac} is higher than σ_{dc}. Since this is a known feature of space charge polarization [36], the conductivity seems to be largely influenced by factors such as crystal size, grain boundary, etc. ZnS nanoparticles with different average grain sizes showed σ_{dc} values much higher than that of bulk ZnS, which is reported to be in the order of 10^{-11} mho m^{-1} [37]. In this present study, the σ_{ac} and σ_{dc} values of the samples are found to be five to six orders of magnitude higher than that of ZnS single crystals [37]. The obtained ε_r value for all the samples are small (6.313 for ZnS(1), 5.857 for ZnS(2), 7.235 for ZnS(3), 6.105 for ZnS(C) and 8.25 for ZnS(B)) when compared to that observed for bulk ZnS (8.76) [38] at room temperature with fixed frequency 1 kHz. These values clearly indicate that the electronic behavior of ZnS QDs is different from that of bulk ZnS structures.

Table 4
Calculated absorption edge wavelength, optical bandgap energy and activation energies.

Sample code	Absorption edge wavelength (nm)	Optical bandgap energy (E_g)	Activation energy	
			ΔE_{ac}	ΔE_{dc}
		eV (±0.011 eV)	eV (±0.008 eV)	eV (±0.008 eV)
ZnS(1)	331.8	3.738	0.499	0.734
ZnS(2)	328.4	3.777	0.469	0.683
ZnS(3)	314.5	3.944	0.435	0.593
ZnS(C)	318.6	3.893	0.457	0.644
ZnS(B)	338.3	3.667	0.562	0.832

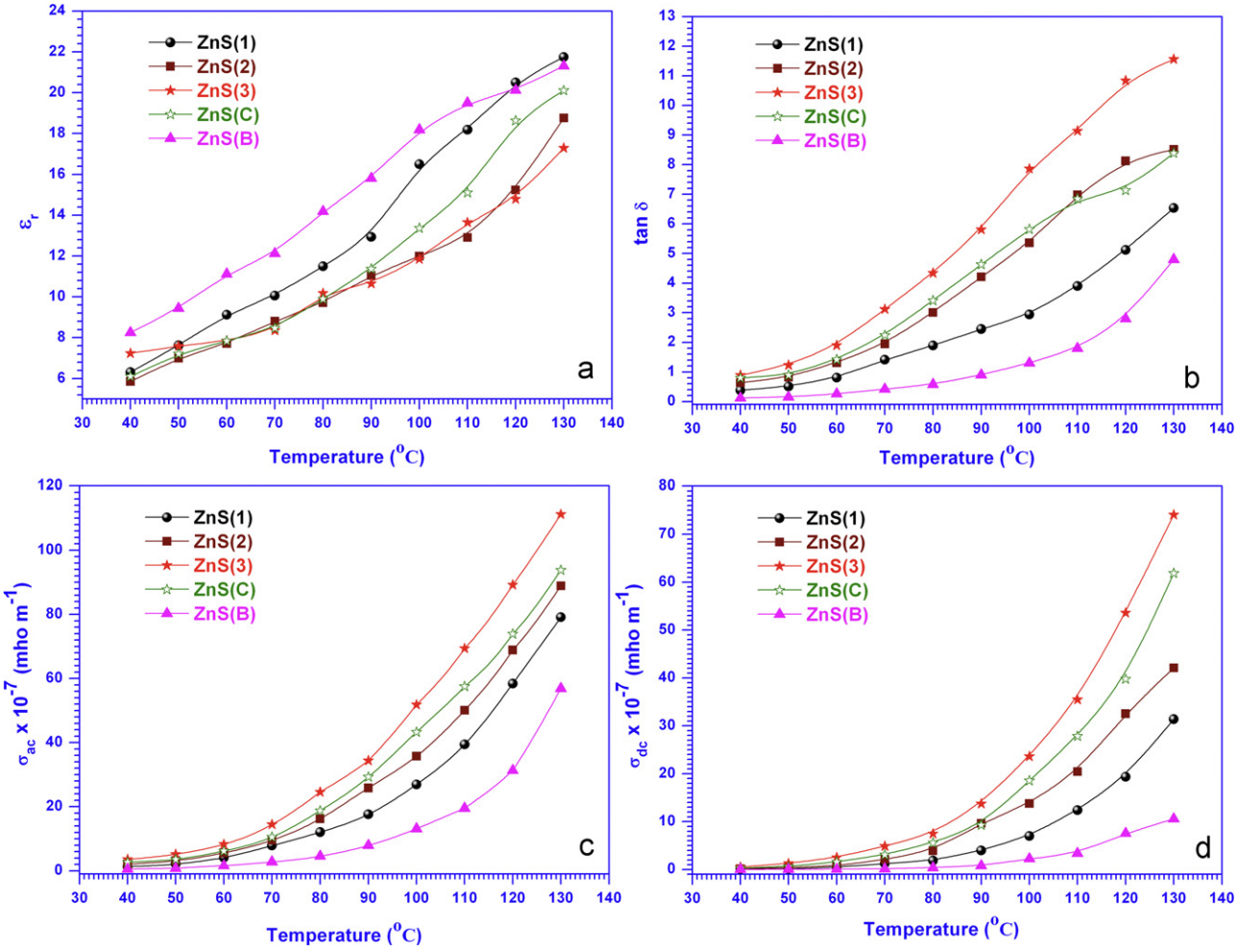

Fig. 7. Temperature dependence of electrical parameters such as (a) dielectric constant ε_r, (b) dielectric loss factor tan δ, (c) AC conductivity σ_{ac} and (d) DC conductivity σ_{dc} for the temperature range of 40–130 °C at a constant frequency (1 kHz). (Colour online.)

The conductivity at the recorded temperature range is found to be in the order of ZnS(3) > ZnS(C) > ZnS(2) > ZnS(1) > ZnS(B). It clearly indicates that the conductivity and the other electrical parameter are size dependent, i.e. the conductivity enhances when the size gets decreased. This observation is rather curious, since, when the band gap increases, one would expect the conductivity to decrease (note that, E_g increases (see Tables 2 and 4) with the decrease in crystallite size). Additionally, it is also an accepted argument that the electrical resistivity of nanocrystalline materials, in general, is higher than that of both conventional coarse grained polycrystalline materials and alloys. When the crystallite size is smaller than the electron mean free path, due to the dominant grain boundary scattering the electrical resistivity is expected to rise as compared to the bulk counterpart. However, in the present case, the observed results are entirely different. The higher conductivity of wide band gap semiconductor (ZnS(3)) as compared to the smaller band gap materials (ZnS(1), ZnS(2), ZnS(C) and ZnS(B)) suggests the presence of donor/acceptor like energy levels [39] with smaller activation energy [40]. In order to understand these, the activation energy (both AC and DC) for conduction was also calculated using the Arrhenius relation. The Arrhenius plots are shown in Fig. 8(a) and (b) and the observed activation energy values are summarized in Table 4. The change in the slope of the curves clearly suggests a dominant effect in conductivity with respect to temperature. The calculated activation energy values suggest that small sized ZnS experience smaller activation barrier for conduction.

The above observation has been already noticed by few other investigators and the concept was explained with interesting theoretical basis [41]. The existing theoretical models can be, in general, categorized in two basic models [42–47], (a) carrier trapping model and (b) dopant segregation model. The former model seems to have made better impact than the latter due to the fact that the latter model could not satisfactorily explain the temperature dependence of conductivity for polycrystalline wide bandgap semiconductor materials. As per the carrier trapping model the presence of defects (or dopants) play a key role. In polycrystalline materials, a significant amount of defects/dopants are trapped and immobilized across the grain boundaries. Therefore significant space near the grain boundary is charge depleted and a potential barrier (activation energy barriers) is thus created across the grain boundary. This barrier impedes the transport of free carriers between the grains. The width of the grain boundary itself implies a barrier, however, since the boundaries are charged with electrons when increasing the temperature electrons get emitted thermionically and tunnel across the thin barriers. Nevertheless, this will happen only when the activation energy barrier of the depletion regions is sufficiently smaller. Mandurah et al. [46,47] have demonstrated that the height and width of this barrier is a function of defect concentration. A pictorial representation of a grain boundary across

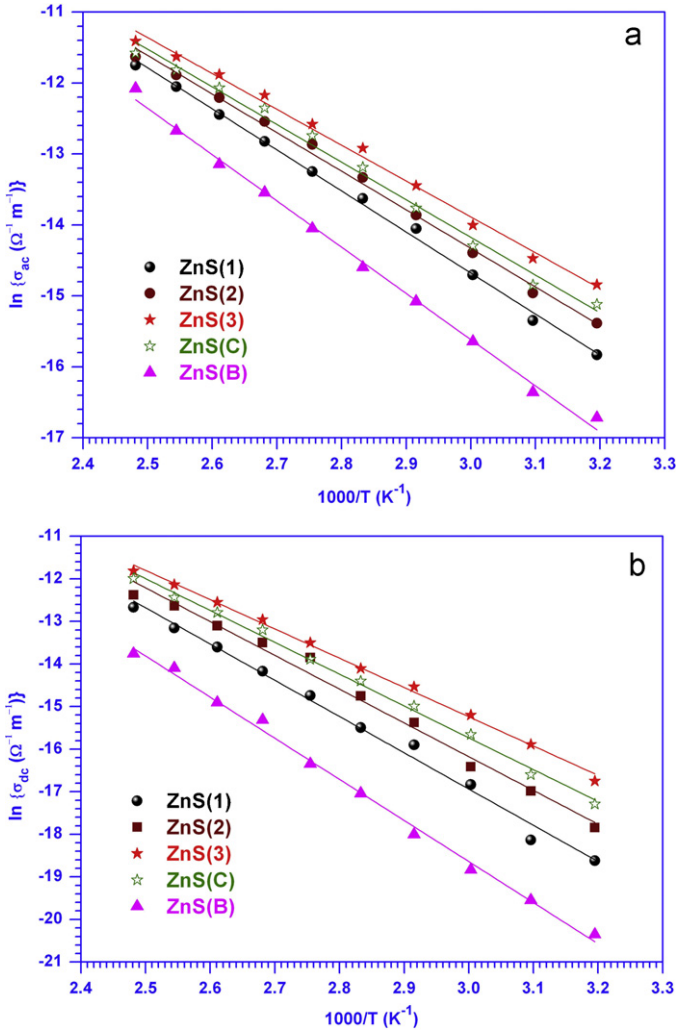

Fig. 8. Arrhenius plots for the analysis of activation energy for (a) AC conductivity and (b) DC conductivity. (Colour online.)

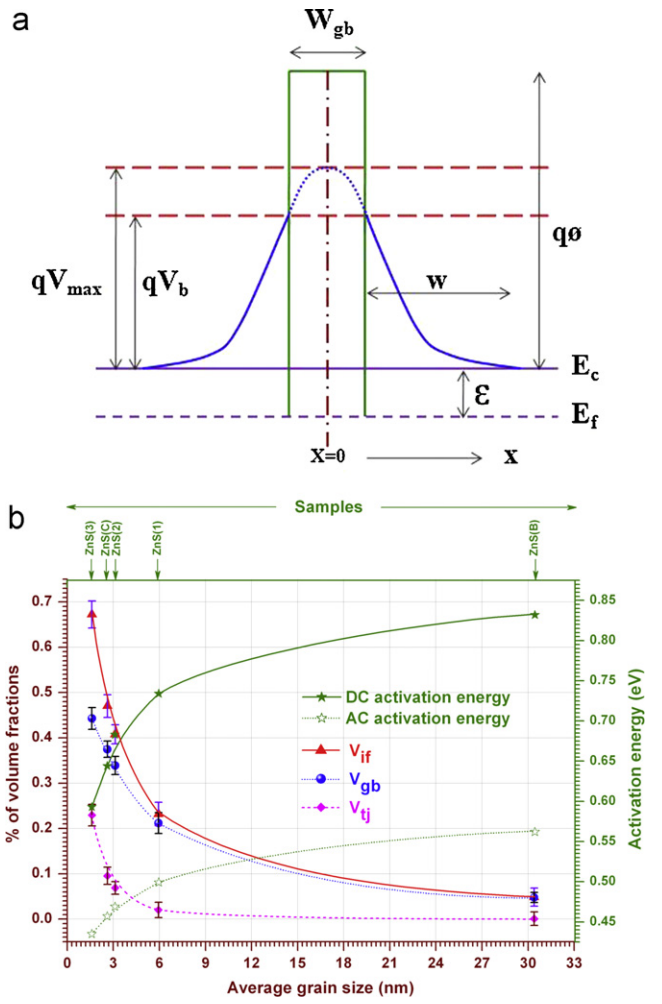

Fig. 9. (a) Pictorial representation of Mandurah et al.'s model for conduction and thermionic emission across the grain boundaries and (b) the plots for volume fraction occupied by grain boundaries (V_{gb}), interfaces (V_{if}) and triple junctions (V_{tj}). The activation energy plots (both AC and DC) are also given in the figure. (Colour online.)

crystallites and potential barrier $qV(x)$ (due to depletion) is given in Fig. 9(a).

The height of the potential energy barrier at any point of x for $(W_{gb}/2) < |x| < (W + (W_{gb}/2))$ is given by

$$qV(x) = \frac{q^2 N_G}{2\varepsilon}\left[\left(W + \frac{W_{gb}}{2}\right) - |x|\right]^2 \quad (7)$$

where, W is the width of the depletion region in one of the sides of the grain boundary, and W_{gb} is the width of the grain boundary itself. The maximum value of $qV(x)$ is given as

$$qV(x)_{max} = \frac{q^2 N_G}{2\varepsilon} W^2 \quad \text{at the point } |x| = \frac{W_{gb}}{2}$$

The width of the charge depleted region W is given by

$$W = \frac{Q_t}{2N_G} \quad (8)$$

Thus the maximum value of the barrier is

$$qV(x)_{max} = \frac{q^2}{8\varepsilon N_G} Q_t^2 \quad (9)$$

where Q_t (cm^{-2}) is the density of trapping states at the grain boundary. N_G is the average defect concentration remaining in the grains after defect segregation at the grain boundaries (for understanding the other variables used in the expression, see Fig. 9(a)). This relation clearly says that, the barrier height and width can be reduced if the immobilized carriers (traps) in the grain boundaries are lesser. Also the higher concentration of mobile defects in the crystallites can largely reduce the barrier and conduction becomes feasible through thermionic emission. The defects might have originated from many factors, such as vacancies, stacking faults, and the excess sulphur presents at the surface.

From these understanding and the lesser activation energy calculated by us (see Fig. 9(b)) it appears to be the smaller size ZnS possesses higher concentration of mobile defects in the crystallites. As we reduce the size of ZnS, a significant fraction of the overall volume is occupied by grain boundaries where the barrier for conduction is very less. The conduction seems to be facilitated by thermionic emission from the grain boundaries. Fig. 9(b) shows the calculated volume fraction occupied by grain boundaries (V_{gb}), interfaces (V_{if}) and triple junction (V_{tj}) of the as-prepared materials. As can be noticed in the figure, when the size is smaller, more volume fraction is occupied by interfaces. At the same time, there is smaller activation energy (both AC and DC) barrier for conduction in materials with higher fraction of such interfaces. When temperature is raised, sine the activation energy barrier is smaller; the charge carriers from the grain boundaries/interfaces get emitted thermionically [48]. Since the thermionic emission promotes local

current, duly supported by very small activation barrier for the conduction of electrons, electrons gets much accelerated across these regions and apparently result in higher conductivity.

4. Conclusion

Five different sizes of ZnS QDs/nanocrystals have been prepared in the present study and the following conclusions have been drawn:

- In solvo-thermal method, microwave assisted heating instead of conventional heating leads to reduction of ZnS size at least >30 times. Microwave heating not only influences the geometry of particles but also the crystal structure of the particles.
- Incorporation of excess Na_2S along with the required amount of reactants results to smaller size of ZnS crystals. However, highly desirable effect can be achieved only when microwave heating source is used instead of conventional heaters.
- NaOH treatment prevents the agglomeration of particles and separates the individual dots to a better extent. In the case of bulk ZnS crystals (conventional method) NaOH treatment is helpful for size reduction also. In the case of QDs of ZnS (microwave heating), NaOH treatment mainly results in the separation of quantum dots.
- The band gap increases as the size of particles decreases. The band gap of bulk ZnS is 3.67 eV. This can be enhanced to 3.9 eV by reducing the ZnS size to ~3 nm.
- High quantum confinement is observed in the case of ZnS with size of ~3 nm where the crystallite size is much smaller than the exciton Bohr radius.
- The activation energy for conduction is smaller in smaller QDs of ZnS. Thus, in spite of the wider band gap, conductivity is higher in these materials. This feature can be understood from the theory of Mandurah et al. model for conduction and thermionic emission mechanism across the grain boundaries.

Acknowledgement

One of the authors (C.K. Mahadevan) thanks the University Grand Commission Hyderabad for the grant of a minor research project.

References

[1] R.H. Mauch, Appl. Surf. Sci. 92 (1996) 589.
[2] S.H. Deulkar, C.H. Bhosale, M. Sharon, J. Phys. Chem. Solids 65 (2004) 1879.
[3] K. Karpiska, M. Godlewski, M. Leskelä, L. Niinistö, J. Alloys Compd. 225 (1995) 544.
[4] L. Qu, Z.A. Peng, X. Peng, Nano Lett. 1 (2001) 333.
[5] T.L. Chu, S.S. Chu, J. Brittand, C. Ferekides, C.Q. Wu, Proceeding of the 22nd IEEE Photovoltaic Specialists' Conference, USA, 1991, p. 1136.
[6] D.V. Petrov, B.S. Santos, G.A.L. Pereira, C.D.M. Donega, J. Phys. Chem. B 106 (2002) 5325.
[7] P. Reiss, J. Bleuse, A. Pron, Nano Lett. 2 (2002) 781.
[8] D. Chen, F. Huang, G. Ren, D. Li, M. Zheng, Y. Wang, Z. Lin, Nanoscale 2 (2010) 2062.
[9] R.E. Anderson, W.C.W. Chan, ACS Nano 2 (2008) 1341.
[10] J. Schoonman, Solid State Ionics 135 (2000) 5.
[11] H.S. Nalwa (Ed.), Handbook of Nanostructured Materials and Nanotechnology, Academic, USA, 2000.
[12] J.C. Bailar, H.J. Emeléus, R. Nyholm, A.F. Trotman-Dickenson (Eds.), Comprehensive Inorganic Chemistry, vol. 2, Pergamon, Oxford, 1973, pp. 268, 560–564, 710.
[13] V.J. Porter, S. Geyer, J.E. Halpert, M.A. Kastner, M.G. Bawendi, J. Phys. Chem. C 112 (2008) 2308.
[14] A.M.A. El-Barry, H.E. Atyia, Physica B 368 (2005) 1.
[15] G.F. Neumark, Phys. Rev. Lett. 62 (1989) 1800.
[16] P.G. Neudeck, R.S. Okojie, L.Y. Chen, Proc. IEEE 90 (2002) 1065.
[17] R.S.S. Saravanan, D. Pukazhselvan, C.K. Mahadevan, Philos. Mag. 91 (2011) 389.
[18] B.D. Cullity (Ed.), Elements of X-ray Diffraction, Addison-Wesley, New York, 1997, p. 102.
[19] R.S.S. Saravanan, D. Pukazhselvan, C.K. Mahadevan, J. Alloys Compd. 509 (2011) 4065.
[20] G. Palumbo, S.J. Thorpe, K.T. Aust, Scr. Metall. Mater 24 (1990) 1347.
[21] H.M. Rietveld, J. Appl. Crystallogr. 2 (1969) 65.
[22] J. Tauc (Ed.), Amorphous and Liquid Semiconductors, Plenum, New York, 1974.
[23] G.P. Joshi, N.S. Saxena, T.P. Sharma, V.S.C. Dixit, K. Mishra, Indian J. Pure Appl. Phys. 41 (2003) 462.
[24] R.K. Nkum, A.A. Adimado, H. Totoe, Mater. Sci. Eng. B 55 (1998) 102.
[25] X. Ren, G. Zhao, H. Li, W. Wu, G. Han, J. Alloys Compd. 465 (2008) 534.
[26] Q. Xiaoa, S. Huangb, J. Zhanga, C. Xiaoa, X. Tan, J. Alloys Compd. 465 (2008) L18.
[27] A.A. Ismail, A. El-Midany, E.A. Abdel-Aal, H. El-Shall, Mater. Lett. 59 (2005) 1924.
[28] H.M. El-Khair, X. Ling, H. Xin-Fan, L. Ming-Hai, C. Kun-Ji, Chem. Phys. Lett. 18 (2001) 616.
[29] L. Dale, D. Huber, Small 1 (2005) 482.
[30] Y. Xiong, J. Zhang, F. Huang, G. Ren, W. Liu, D. Li, C. Wang, Z. Lin, J. Phys. Chem. C 112 (2008) 9229.
[31] B. Liu, J. Li, Li. Jing-hong, Chin. J. Chem. Phys. 20 (2007) 495.
[32] H. Landolt, R. Bornstein (Eds.), Numerical Data and Functional Relationships in Science and Technology, Springer-Verlag, Berlin, 1999.
[33] S.V. Gaponenko (Ed.), Optical Properties of Semiconductor Nanocrystals, Cambridge University Press, Cambridge, 1998.
[34] L. Bornstein, O. Madelung (Eds.), Numerical Data and Functional Relationships in Science and Technology. Group III: Crystal and Solid State Physics, Intrinsic Properties of Group IV Elements and III–V, II–VI, and IV Compounds, vol. 22A, Springer Verlag, Berlin, 1987, p. 168.
[35] D. Vollath (Ed.), Nanomaterials an Introduction to Synthesis, Properties and Applications, Wiley-VCH, Weinheim, 2008.
[36] J.R. Macdonald, Phys. Rev. 92 (1953) 4.
[37] E. Birringuier, Philos. Mag. B 75 (1997) 209.
[38] B. Ray (Ed.), II–VI Compounds, Pergamon Press, Oxford, 1998.
[39] L. Brus, J. Phys. Chem. 90 (1986) 2555.
[40] C.-W. Nan, T. Schope, S. Holten, H. Kleim, R. Birringer, J. Appl. Phys. 85 (1999) 7735.
[41] V. Biju, M.A. Khadar, Mater. Res. Bull. 36 (2001) 21.
[42] M.M. Mandurah, K.C. Saraswat, T.I. Kamins, J. Electrochem. Soc. 126 (1979) 1019.
[43] J.Y.W. Seto, J. Appl. Phys. 46 (1975) 5247.
[44] N.C.C. Lu, L. Gerzberg, J.D. Meindl, IEEE Electron Device Lett. EDL-1 (1980) 36.
[45] M.E. Cowher, T.O. Sedgwick, J. Electrochem. Soc. 119 (1978) 1565.
[46] M.M. Mandurah, K.C. Saraswat, T.I. Kamins, IEEE Trans. Electron Devices ED-28 (1981) 1161.
[47] M.M. Mandurah, K.C. Saraswat, T.I. Kamins, IEEE Trans. Electron Devices ED-28 (1981) 1171.
[48] V. Snejdar, J. Jerhot, Thin Solid Films 37 (1976) 303.